Exploration of the Method of Weighted Residuals in Numerical Models of Solidifying Sediment Flows

Dieter Issler*† and Shinji Sassa†

May 15, 2015

Abstract

Numerical modeling of solidifying sediment flows poses a computational challenge because of the inherent three-dimensionality of the phenomenon: Despite the shallowness of the flow, the traditional method of depth-averaging is inadequate because the vertical distribution of sediment plays a central dynamical role and also affects the velocity profile. In 3D simulations, the large vertical gradients require fine meshes and short time steps. This report explores whether the Method of Weighted Residuals (MWR) can be used to reduce the problem to 2D while retaining essential information on the bed-normal profiles of velocity and concentration.

The MWR is first applied to strongly simplified flow problems. In the case of an infinitely long film of linearly viscous material starting from rest on an inclined plane, traditional depth-averaging is a special case of the MWR, with just a single basis function (a parabola) and the constant function as weight function. Comparison with the exact solution shows that this approximation approaches equilibrium too rapidly because the shear rate at the bed is strongly underestimated in the start-up phase. Much better agreement with the exact solution results if one uses a parabolic weight function instead. One obtains even higher accuracy if one uses four basis functions that capture the temporal variability of the velocity profile. The MWR thus shows promise for models of one-component flows with relatively simple rheological laws.

The present report summarizes the theory of sediment flows as two-component mixtures (ambient water and particles) in the case of low Stokes number so that the motion of the particles relative to the fluid can be approximated by a single settling velocity that depends on the local concentration according to the well-established Richardson–Zaki correlation. We find, however, that the strong non-linearity of this relation increases the computational load by several orders of magnitude over that for a fully depth-resolved computation. So far, no viable alternative approach has been found. However, problems with moderate non-linearity and a small number of basis functions can be solved efficiently by the MWR.

*Natural Hazards Division, Norwegian Geotechnical Institute, Postboks 3930 Ullevål Stadion, 0806 Oslo, Norway

†Soil Dynamics Group, Port and Airport Research Institute, 3-1-1 Nagase, Yokosuka-shi, Kanagawa-ken 239-0826, Japan

1 Motivation and scope of this work

Hyperconcentrated sediment flows are an important agent of mass wasting along virtually all coasts of the world's oceans. In addition, they also can have important consequences for human life and activities in coastal areas because they may destabilize the coastline, generate tsunamis or destroy seafloor installations. For this reason, prediction of their run-out distance, flow depth and velocity is an important task.

While the sediment is flowing, it is fully liquefied, i.e., the volumetric concentration, c, is below a critical value of the order of $c_{\mathrm{cr}} \approx 0.6$. Above this threshold, sediment grains are permanently in contact with other grains so that a grain skeleton with stiffness and effective stress develop and become important. This indicates that the flowing sediment can be treated as a Newtonian fluid with concentration-dependent viscosity and density, with corrections to the stress tensor at concentrations approaching c_{cr}.

Due to their higher density, grains settle under the action of gravity. The concentration near the bottom of the flow increases and eventually reaches c_{cr}, upon which an immobile deposit forms. Eventually, all sediment settles out and the flow comes to a halt. (Possibly, the water that originally was pore fluid continues to flow for some distance because of its momentum.) As discussed by Sassa & Sekiguchi (2010), there should be a thin transitional layer in which the sediment concentration is so high that the material has stiffness, but the effective stress is still zero. Also note that the settling of grains causes pore water to migrate upwards, thus contributing to the fluidization of the upper layers of the flow.

The majority of mathematical models of sediment flows neglect the sedimentation process even though it is obviously an essential ingredient when it comes to calculating the run-out distance. One of the models developed to account for this effect is LIQSEDFLOW (Sassa & Sekiguchi, 2010), which has been tested successfully against carefully measured laboratory sediment flows. LIQSEDFLOW is formulated as a two-dimensional Eulerian model in a vertical plane, using the Volume-of-Fluid (VOF) technique to track the migration of the solidification front in space and time.

Despite its success in reproducing the phenomenon of sedimentation and flow arrest, application of LIQSEDFLOW to real-world cases is hampered by the fact that lateral spreading of the flow or lateral variation of the topography cannot be taken into account in its present formulation. Extending the code to three dimensions is, in principle, quite straightforward, but the numerical effort required for simulations will become very significant, even with today's powerful computers. For numerical reasons, the number of cells of the computational grid cannot be kept tractable by making the cells larger in the horizontal dimensions—they would become "pizza boxes" and the accuracy of the computation would suffer greatly, or else very small time steps would have to be used.

The traditional remedy for this problem is to use depth-averaging, i.e., the governing equations are integrated over the bed-normal (or vertical) direction, thereby reducing the dimensionality from 2 or 3 to 1 or 2 and introducing an additional field variable, namely the instantaneous local flow depth. This approximation is known to be suitable for shallow flows like granular avalanches or density current; sediment flows usually are shallow, with an aspect ratio of the order of 10^{-2}. However, in the course of the depth averaging, one loses information about the shape of the velocity and concentration profiles, which are central to LIQSEDFLOW. Depth-averaged models incorporating boundary-related effects like deposition or erosion need to make ad-hoc assumptions about the shape of the profiles in order to close their equations; an important and very well explained example is the model of self-igniting turbidity currents by Parker *et al.* (1986).

A possible way out of this dilemma may be to include the information on the bed-normal dimension in an approximate way by expanding the dynamical fields in terms of a set of basis functions along the bed-normal direction and truncating the series after the first few terms. The first application of the so-called Kantorovich technique [a special case of the Method of

Weighted Residuals (MWR)] to gravity mass flows known to the authors was the powder-snow avalanche model by Scheiwiller & Hutter (1982); Scheiwiller (1986). Later applications are, e.g., in the field of film flow dynamics by Ruyer-Quil & Manneville (1998, 2000, 2002); Scheid *et al.* (2006). In this way, one needs to solve $4N$ coupled partial differential equations (PDEs) in 1 or 2 dimensions instead of 4 PDEs in 2 or 3 dimensions if one uses N basis functions. In addition, the "pizza-box" constraint does not apply and one can use larger cells and correspondingly longer time steps. Anticipating $N = 3 \ldots 5$ while a full 2D/3D computation would require approximately 30 cells in the bed-normal direction, we expect the computational effort to be reduced by one to two orders of magnitude.

The purpose of the present report is to document our exploration of this topic. Unfortunately, after promising beginnings, it turned out that the strong non-linearity of the settling velocity renders the MWR unsuitable for this type of problem. We explain the method first in a simplified setting, namely a Newtonian fluid on an inclined plane, in sec. 2. Sections 3.1 and 3.2 present the equations for the sediment flow model. Section 4 describes the expansion in the bed-normal direction more precisely, and then shows why the MWR does not provide a practical solution for highly non-linear equations. Finally, sec. 5 contains our (preliminary) conclusions and suggestions for future work.

2 The Method of Weighted Resiudals applied to simple flow models

As a warm-up exercise, we study the MWR technique for simple, one-component flow models. We consider Newtonian and frictional-collisional fluids because their equilibrium velocity profiles are easily computed and they also have important practical applications. Moreover, the time evolution of the velocity profile of a Newtonian fluid on an inclined plane, starting from rest, can be expressed as an infinite series in the so-called infinite-slope approximation; this makes it possible to compare the results from an MWR model to the exact solution.

2.1 Equations and assumptions

We start from the mass and momentum balance equations in 2D (x and z coordinates in a vertical plane), assuming a uniform slope for the time being. We also make the hydrostatic pressure approximation, even though the MWR technique would be ideally suited for going beyond this central approximation in depth-averaged flow models. Instead, we put the emphasis on obtaining better, time-dependent approximations for the velocity profile. Assuming an incompressible fluid, we write the balance equations for mass and momentum in conservative form as

$$\partial_x u + \partial_z w = 0, \tag{1}$$

$$\partial_t u + \partial_x(u^2) + \partial_z(wu) = g_x - \partial_x \hat{p} + \partial_x \hat{\sigma}_{xx} + \partial_z \hat{\sigma}_{xz}. \tag{2}$$

$$\partial_t w + \partial_x(uw) + \partial_z w^2 = g_z - \partial_z \hat{p} + \partial_x \hat{\sigma}_{zx} + \partial_z \hat{\sigma}_{zz}. \tag{3}$$

Here, $\hat{p}$ and $\hat{\sigma}$ are the pressure and the deviatoric stress per unit mass, respectively (the caret $\hat{}$ indicates division by the density). We assume the simple constitutive law of an incompressible Newtonian fluid,

$$\hat{\sigma}_{ij} = 2\nu \left(D_{ij} - \frac{1}{2}\delta_{ij} D_{kk} \right). \tag{4}$$

$D_{ij} \equiv \frac{1}{2}(\partial_j u_i + \partial_i u_j)$ is the symmetric strain-rate tensor. Note that we use Einstein's summation convention throughout this report, i.e., repeated indices are understood to be summed over unless they are surrounded by small parentheses. Thus $D_{kk} = D_{xx} + D_{zz}$ in 2D. Note that eq. (1) can be used to transform the advective terms in eqs. (2) and (3) into their non-conservative forms $u\partial_x u + w\partial_z u$ and $u\partial_x w + w\partial_z w$, respectively.

In the shallow-water approximation for flows whose vertical length scale is much smaller than their horizontal length scale, $H = \epsilon L$ with $\epsilon \ll 1$, u and ∂_z can be considered of order 1 while w, ∂_t and ∂_x are of order ϵ. g_x and g_z, the slope-parallel and slope-normal components of the gravitational acceleration g, as well as $\hat{p}$ and $\hat{\sigma}$ are considered to be of order 1. Both terms in the mass balance equation are of order ϵ. To order zero, the x-momentum equation reduces to the balance between gravity along the slope and the shear stress gradient, and the z-momentum equation to the balance between overburden weight and pressure. All terms on the left-hand side are of order ϵ in eq. (2) and should be kept, but in eq. (3) they are of order ϵ^2 and can be dropped in our approximation. This leads to a hydrostatic pressure distribution in the flow. Introducing the flow depth h as a new variable, we get

$$\hat{p}(x, z, t) \approx -[h(x, t) - z]g_z = (1 - \zeta)hg_z. \tag{5}$$

In the case of a Newtonian fluid, the only non-zero components of the deviatoric stress are

$$\hat{\sigma}_{xz}(x, z, t) = \hat{\sigma}_{zx}(x, z, t) \approx \nu\dot{\gamma}. \tag{6}$$

We defined the non-dimensional slope-normal coordinate by $\zeta \equiv z/h$ and $\dot{\gamma}$ as a shorthand for $\partial_z u$. Equation (6) is an approximate equation because we neglect shear stress contributions from the shear deformation $\partial_x w$, which is of order ϵ^2. ν is the kinematic viscosity of the fluid.

For a frictional-collisional fluid, we can write the stress tensor as

$$\hat{\sigma}_{xx} = -p_e - p_u - (\nu_n - \nu_d)\dot{\gamma}^2, \tag{7}$$

$$\hat{\sigma}_{zz} = -p_e - p_u - \nu_n\dot{\gamma}^2, \tag{8}$$

$$\hat{\sigma}_{xz} = \mu\hat{\sigma}_{zz} + \nu_s\dot{\gamma}^2. \tag{9}$$

These equations result when a more general and manifestly covariant formulation (Irgens, 2004) is evaluated in this configuration. p_e and p_u are the effective pressure (mediated by enduring inter-particle contacts) and the pore pressure, respectively. The model accommodates normal-stress differences (if $\nu_d \neq 0$). The consistencies ν_n, ν_s and ν_d have units m^2 and are expected to scale with the square of the mean particle diameter. They must also have a strong dependence on the particle concentration (Pasquarell *et al.*, 1988; Campbell & Gong, 1986), but we assume the density to be constant at this stage of the development.

The boundary conditions to be imposed on the velocity are

$$u(x, 0, t) = w(x, 0, t) = 0, \qquad \partial_z u(x, h, t) = \partial_z w(x, h, t) = 0. \tag{10}$$

The first is the no-slip condition at the bed, whereas the second is related to the assumption that the flow surface is stress-free, $\hat{p}(x, h, t) = \hat{\sigma}_{jk}(x, h, t) = 0$. There is an additional, kinematic, boundary condition at the flow surface to reflect the fact that this is a material boundary:

$$\partial_t h(x, t) + u(x, h, t)\partial_x h(x, t) - w(x, h, t) = 0. \tag{11}$$

2.2 Expansion of the fields and depth-integration

First, we integrate the mass balance equation over the z-direction to obtain

$$\partial_x \int_0^h u(x, z, t)\mathrm{d}z + w(x, h, t) - w(x, 0, t) - u(x, h, t)\partial_x h = 0.$$

Due to the boundary conditions, $w(x, 0, t) = 0$. According to the kinematic boundary condition (11), the second and last term combine to $\partial_t h(x, t)$. The integral equals $h\bar{u}(x, t)$, $\bar{u}$ being the depth-averaged velocity. The mass balance thus is transformed into an evolution equation for the flow depth:

$$\partial_t h + \partial_x(h\bar{u}) = 0. \tag{12}$$

Before proceeding to the x-momentum balance equation, we introduce an expansion of the velocity fields u in terms of a complete set of orthonormal basis functions $\phi_i(\zeta),\ i = 0, 1, 2\ldots$ with the properties

$$\langle \phi_j, \phi_k \rangle \equiv \int_0^1 \phi_j(\zeta)\phi_k(\zeta)\mathrm{d}\zeta = \delta_{jk}, \tag{13}$$

$$\phi_k(\zeta)\phi_k(\zeta') = \delta(\zeta - \zeta'). \tag{14}$$

Note the use of the Einstein summation convention in eqn. (14). We write the expansion as

$$u(x, z, t) = v_j(x, t)\phi_j(\zeta). \tag{15}$$

In order to satisfy the boundary conditions, the basis functions are to be constructed such that $\phi_j(0) = \phi_j'(1) = 0$ for all j. The depth-averaged velocity can then be expressed as

$$\bar{u}(x, t) = \frac{1}{h} v_i(x, t) \int_0^{h(x,t)} \phi_i(\zeta) h \mathrm{d}\zeta \equiv a_i v_i(x, t). \tag{16}$$

The coefficients a_i are fixed numbers that can be computed once the basis functions $\phi_i(\zeta)$ are defined.

If one treats the x-momentum balance equation in the same way, again making use of the kinematic boundary condition, one obtains

$$\partial_t(h\bar{u}) + \partial_x\left(h\overline{u^2}\right) = hg_x + \partial_x\left(\frac{h^2}{2}g_z\right) - \nu\partial_z u|_{z=0}. \tag{17}$$

One may substitute the expansion in terms of basis functions into $\bar{u}$, $\overline{u^2}$ and $\partial_z u|_{z=0}$, but in this way one obtains only one evolution equation for all the fields $v_i(x, t)$. A method for obtaining n evolution equations for n modes consists in applying the depth integration, not to the original momentum balance equation, but to the momentum balance equation (in non-conservative form) multiplied by weight functions $W_j(\zeta)$, which one has to choose suitably. The orthonormality property (13) suggests to use the basis functions themselves for this purpose, $W_j(\zeta) = \phi_j(\zeta)$. This indeed isolates the time derivative of a single mode field in the first term:

$$\int_0^1 \phi_i(\zeta)\phi_j(\zeta)\partial_t v_j(x, t)\mathrm{d}\zeta = \delta_{ij}\partial_t v_j(x, t) = \partial_t v_i(x, t).$$

Except for the last term on the left-hand side, this works as expected:

$$\int_0^1 \phi_i(\zeta)\phi_j(\zeta)\phi_k(\zeta)v_j(x, t)\partial_x v_k(x, t)\mathrm{d}\zeta = a_{ijk}v_j(x, t)\partial_x v_k(x, t),$$

$$\int_0^1 \phi_i(\zeta)g_x\mathrm{d}\zeta = a_i g_x,$$

$$-\int_0^1 \phi_i(\zeta)\partial_x(-hg_z)(1 - \zeta)\mathrm{d}\zeta = (a_i - b_i)\partial_x(hg_z),$$

$$\int_0^1 \phi_i(\zeta)\partial_z[\nu\partial_z v_j(x, t)\phi_j(\zeta)]\mathrm{d}\zeta = c_{i,j}\frac{\nu}{h^2}v_j(x, t),$$

We defined coefficients representing integrals over one, two and three basis functions:

$$a_i = \int_0^1 \phi_i(\zeta)\mathrm{d}\zeta, \tag{18}$$

$$b_i = \int_0^1 \zeta\phi_i(\zeta)\mathrm{d}\zeta, \tag{19}$$

$$c_{ij} = \int_0^1 \phi_i(\zeta)\phi_j''(\zeta)\mathrm{d}\zeta, \tag{20}$$

$$a_{ijk} = \int_0^1 \phi_i(\zeta)\phi_j(\zeta)\phi_k(\zeta)\mathrm{d}\zeta, \tag{21}$$

Once the basis functions are chosen, these coefficients can be computed before the simulation; they are constants. The ζ-dependence has been integrated out, the v_j are fields that depend only on x and t.

The stumbling block is the advective term that contains the vertical velocity w. If one wants to go beyond the hydrostatic-pressure approximation, one has to expand $w(x,z,t) = q_i(x,t)\psi_i(\zeta)$ (presumably expanding in a different set of basis functions from the ϕ_i used for u) and use the full z-momentum equation. While this appears feasible and should be interesting, we try to keep the model as simple as possible by eliminating the field w. To this end, we integrate the incompressibility equation $\partial_z w = -\partial_x u$ from 0 to z and obtain

$$w(x,z,t) = w(x,0,t) + \int_0^z \partial_{z'} w(x,z',t)\mathrm{d}z' = -\int_0^z \partial_x u(x,z',t)\mathrm{d}z'. \tag{22}$$

Thus the integral of the third term multiplied by the weight function ϕ_i becomes

$$\begin{aligned}\int_0^1 \phi_i(\zeta) w(x,z,t)\partial_z u(x,z,t)\mathrm{d}\zeta &= -\frac{1}{h}\partial_x v_k v_j \int_0^1 \phi_i(\zeta) h\Phi_k(\zeta)\phi_j'(\zeta)\mathrm{d}\zeta \\ &= -d_{jik} v_j \partial_x v_k,\end{aligned} \tag{23}$$

where $\Phi_k(\zeta)$ is the anti-derivative of $\phi_k(\zeta)$ and

$$d_{ijk} = \int_0^1 \phi_i'(\zeta)\phi_j(\zeta)\Phi_k(\zeta)\mathrm{d}\zeta = \int_0^1 \phi_i'(\zeta)\phi_j(\zeta)\int_0^\zeta \phi_k(\zeta')\mathrm{d}\zeta'\mathrm{d}\zeta. \tag{24}$$

Putting all this together, we arrive at

$$\partial_t v_i + (a_{ijk} - d_{ijk}) v_j \partial_x v_k = a_i g_x + (a_i - b_i)\partial_x(h g_z) - c_{ij}\frac{\nu}{h^2} v_j, \tag{25}$$

2.3 Relation to traditional depth-averaged models

One may suspect that the usual depth-averaging corresponds to choosing some function $\phi_0(\zeta)$ and dropping all other terms of the expansion, but it turns out that things are not that simple. For example, with a uniform profile, $\phi_0 = 1$ (disregarding the desired boundary conditions), v_0 becomes $\bar{u}$, the depth-averaged velocity. Of the coefficients, only $a_0 = 1$, $b_0 = \frac{1}{2}$ and $a_{000} = 1$ survive, leading to the following momentum balance equation in x-direction:

$$\partial_t \bar{u} + \bar{u}\partial_x \bar{u} = g_x - \frac{1}{2}\partial_x(h g_z).$$

The bed shear stress is lost in the process because there is no shear inside the flow, only slip at the bed, for which no shear stress is defined in the model. A better choice for a Newtonian fluid is to take a parabolic profile function, $\phi_0(\zeta) = \sqrt{15/8}\,(2\zeta - \zeta^2)$, from which one gets the following values for the coefficients:

$$a_0 = \frac{\sqrt{30}}{6}, \qquad b_0 = \frac{5\sqrt{30}}{48}, \qquad c_{0,0} = -\frac{5}{2}, \qquad a_{000} = \frac{3\sqrt{30}}{14}, \qquad d_{0,0,0} = \frac{11\sqrt{30}}{224}.$$

Substituting this back into the x-momentum balance (25), we find

$$\partial_t v_0 + \frac{37\sqrt{30}}{224} v_0 \partial_x v_0 = \frac{\sqrt{30}}{6} g_x + \frac{3\sqrt{30}}{16}\partial_x(h g_z) - \frac{5}{2}\nu\frac{v_0}{h^2}.$$

Before this equation can be compared to standard depth-averaged formulations in a meaningful way, the function $v_0(x,t)$ must be expressed in terms of $\bar{u}$, which is given, in our approximation, by $\bar{u} = a_0 v_0$. So we obtain

$$\frac{6}{5}\partial_t \bar{u} + \frac{6}{5}\left(1 - \frac{1}{112}\right)\bar{u}\partial_x \bar{u} = g_x + \frac{9}{8}\partial_x(h g_z) - 3\nu\frac{\bar{u}}{h^2}. \tag{26}$$

Comparing this to the traditional depth-averaged equation,

$$\partial_t \bar{u} + \frac{6}{5}\bar{u}\partial_x \bar{u} = g_x + \partial_x(hg_z) - 3\nu\frac{\bar{u}}{h^2},$$

we see that the exact equilibrium solution for simple shear flow on an incline in the infinite-slope approximation is recovered, while the relaxation time is about 20% longer than in the traditional depth-averaged model. We will see later that the equation derived by the MWR with parabolic profile both as basis function and weight function actually provides a better approximation of the start-up dynamics of the system on an inclined plane than the usual depth-averaged equation.

The effect of spatial pressure gradients is enhanced by some 10% relative to the source terms on the right-hand side. However, if we consider a frictionless dam-break problem on a horizontal plane, eqn. (26) reduces to

$$\partial_t \bar{u} + \frac{111}{112}\bar{u}\partial_x \bar{u} = \frac{15}{16}\partial_x(hg_z).$$

The pressure-gradient term is somewhat suppressed compared to the usual shallow-water approximation so that the wave speeds will be underpredicted by about 3%. This is perhaps not so surprising, given that the parabolic velocity profile is not the correct solution in this case.

The reason for the discrepancy between the two approximations is the choice of weight function: The usual depth averaging can be considered as the MWR with the weight function $W_0(\zeta) = 1$. Choosing $W_0(\zeta) = \phi_0(\zeta)$ instead emphasizes the contribution of that particular basis function. In the start-up phase, the parabolic profile is closer to the exact solution than the uniform profile; in particular, the large shear rate at the bottom and thus the shear stress are captured more closely.

2.4 Choice of basis functions

Two questions of immediate practical importance are how to best choose the basis functions and how many terms are needed to obtain a good approximation of the (unknown) exact solution. Evidently, the answer will depend on the settings of the problem and on the requirements with respect to accuracy so that a general answer can hardly be given. In this context, it should therefore be useful to study a few classes of basis functions to develop a certain degree of intuition for these issues. The basis functions should be chosen such that they respect the boundary conditions of the system under study and that the first few terms of the expansion already give a good approximation.

2.4.1 Finite-difference formalism by MWR

The MWR approach comprises finite-difference schemes as a special case. We briefly describe our first attempt because it is instructive to see why it fails. Divide the flow depth into n intervals, which we assume to be of equal length for simplicity, and set

$$\phi_j(\zeta) = \begin{cases} (15n/8)^{1/2}\,\Theta(\zeta)\,\Theta(\frac{1}{n}-\zeta)\,\left(1-(1-n\zeta)^2\right) & j=1, \\ n^{1/2}\,\Theta(\frac{j}{n}-\zeta)\,\Theta(\zeta-\frac{j-1}{n}) & j>1. \end{cases} \tag{27}$$

$\Theta(x) = 1$ for $x > 0$ and 0 else. ϕ_1 is constructed so as to satisfy the boundary condition at $z = 0$, and ϕ_n satisfies the one at $z = h$, being constant. However, these basis functions are not continuous at the endpoints of their support intervals, though they are differentiable because the limit of the derivative is the same on both sides of the discontinuity, namely 0 (except at $\zeta = 0$, where there is no other side). Fields constructed from these basis functions will also be discontinuous at $\zeta = j/n$, but twice continuously differentiable everywhere, except at $\zeta = 1/n$ where the second derivative jumps from $-(\frac{15}{2}n^5)^{1/2}$ to 0. This is relevant because such derivatives appear in c_{ij} and d_{ijk}. Having disjoint support, these basis functions are manifestly orthogonal, and one easily verifies that they are orthonormal with the prefactors given above.

An immediate consequence of the basis functions having disjoint support is that integrals with basis functions with different indices vanish identically. The equations for different flow layers thus are discoupled, except for a weak indirect coupling through the mass balance equation, where all layers contribute to h, which in turn appears in the pressure term of the x-momentum balance. A consequence of the basis functions being constant inside their support is that all coefficients containing ζ-derivatives vanish identically except in the bottom layer. The most important victim of this is the viscous friction term.

This looks surprising at first, but the reason lies in the pathology of the chosen basis: While any function can be approximated to arbitrary precision in this basis, the derivative remains zero throughout. We should have verified at the beginning whether this set of basis functions is complete or not. Indeed, for any given n this is a finite set of functions and as such cannot possibly span an infinite-dimensional vector space of functions.

A better approach results if we choose the basis and weight functions as

$$\phi_j(\zeta) = \begin{cases} n\zeta - j + 1, & \frac{j-1}{n} < \zeta < \frac{j}{n} \\ j + 1 - n\zeta, & \frac{j}{n} < \zeta < \frac{j+1}{n} \\ 0, & \text{else.} \end{cases} \tag{28}$$

These basis functions are not differentiable at the points $\frac{j-1}{n}$, $\frac{j}{n}$ and $\frac{j+1}{n}$, and they are not orthonormal either:

$$\int_0^1 \phi_j(\zeta)\phi_k(\zeta)\mathrm{d}\zeta = \frac{2}{3n}\delta_{jk} + \frac{1}{6n}(\delta_{j,k+1} + \delta_{j,k-1}). \tag{29}$$

In order to satisfy the boundary conditions at $\zeta = 0$ and $\zeta = 1$, we have to impose $v_0(x,t) \equiv 0$ and $v_n(x,t) \equiv v_{n-1}(x,t)$. The depth-averaged velocity is given by

$$\bar{u}(x,t) = \frac{1}{n}\sum_{j=1}^{n} v_j(x,t).$$

When we integrate the momentum balance equation weighted with $\phi_j(\zeta)$, only the coefficient fields v_{j-1}, v_j and v_{j+1} contribute:

$$\begin{aligned} \partial_t v_j \;+\; & \frac{1}{4}\partial_t(v_{j-1} + v_{j+1}) + \frac{3}{4}v_j\partial_x v_j \\ & + \frac{1}{8}[v_j\partial_x(v_{j-1} + v_{j+1}) + (v_{j-1} + v_{j+1})\partial_x v_j + v_{j+1}\partial_x v_{j+1} + v_{j-1}\partial_x v_{j-1}] \\ = \; & hg_x + \partial_x\left(\frac{h^2}{2}g_z\right) - \frac{3n}{4}\frac{\nu}{h}(v_{j+1} - v_{j-1}) \end{aligned} \tag{30}$$

In this formulation, the shear stress is retained in the equations. The equation shows that the coefficient function v_j is directly coupled to its neighbors v_{j-1} and v_{j+1} and that the difference $v_{j+1} - v_{j-1}$ must decrease as $1/n$ if the number of nodes is increased.

We will not dwell on this approach further.

2.4.2 Polynomials

It is known that the polynomials $p(x) = \sum_{j=0}^{\infty}\alpha_j x^j$ on a finite interval form an (infinite-dimensional) complete basis in some space of functions that contains all functions we are interested in at present, namely continuously differentiable functions on $[0,1]$ with $f(0) = f'(1) = 0$. These functions form a linear subspace. All polynomials in this set must have $\alpha_0 = 0$ to fulfill $p(0) = 0$. A linear polynomial $p_1(x) = \alpha_1 x$ cannot have $p_1'(1) = 0$. We assume without formal proof that the polynomials of degree 2 and higher span this space. An orthonormal

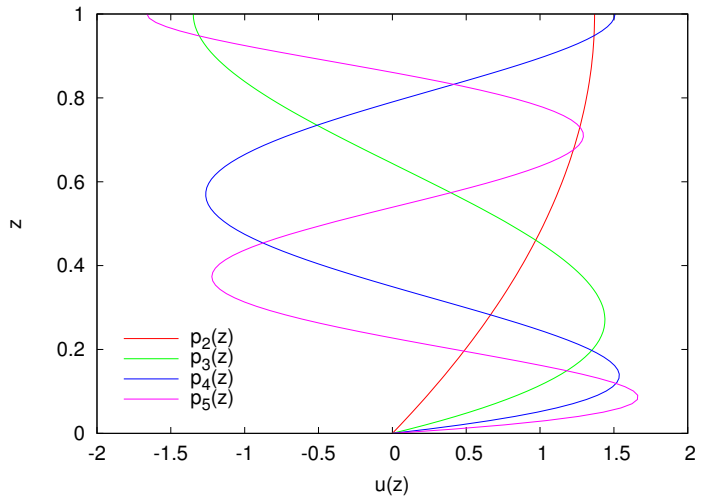

Figure 1: The first four basis functions of the polynomial basis.

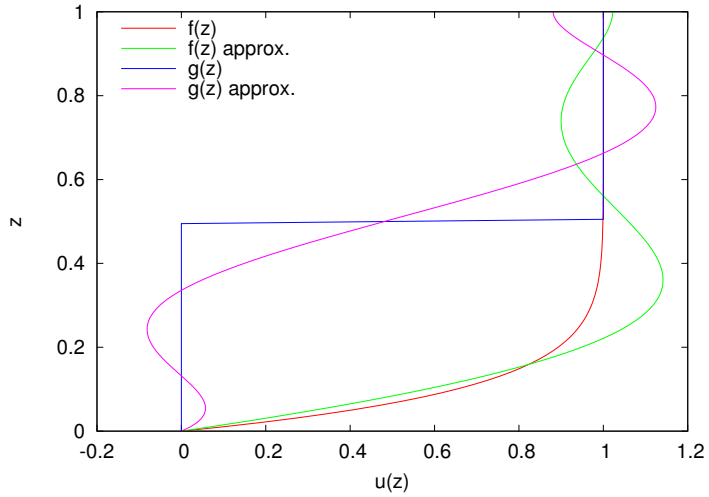

Figure 2: Two selected functions and their approximation by superpositions of the polynomials $p_2(\zeta), \ldots, p_5(\zeta)$.

set $\{p_j(x), j > 1\}$ of candidate basis functions is easily built up, starting from the quadratic polynomial $p_2(\zeta) = \alpha_{2,1}\zeta + \alpha_{2,2}\zeta^2$. One finds $\alpha_{2,1} = -2\alpha_{2,2} = \sqrt{15/2}$. Generally, the condition $p_n'(1) = 0$ imposes $\alpha_{n,n} = -\sum_1^{n-1} j\alpha_{n,j}$, and the $n-2$ conditions $\int_0^1 p_k(\zeta)p_n(\zeta)\mathrm{d}\zeta = 0$ determine $\alpha_{n,2}, \ldots, \alpha_{n,n-1}$. $\alpha_{n,1}$ is fixed by the normalization condition $\int_0^1 p_n^2(\zeta)\mathrm{d}\zeta = 1$. The four lowest-order polynomials of this basis are as given below and shown in fig. 1:

$$p_2(\zeta) = \frac{\sqrt{15}\zeta}{2\sqrt{2}}(2-\zeta) \tag{31}$$

$$p_3(\zeta) = \frac{\sqrt{21}\zeta}{2\sqrt{26}}(26-61\zeta+32\zeta^2) \tag{32}$$

$$p_4(\zeta) = \frac{3\zeta}{2\sqrt{286}}(286-1431\zeta+2072\zeta^2-910\zeta^3) \tag{33}$$

$$p_5(\zeta) = \frac{\sqrt{3}\zeta}{2\sqrt{22}}(242-2017\zeta+5384\zeta^2-5730\zeta^3+2112\zeta^4) \tag{34}$$

As a test of the potential of this basis, let us try to approximate the functions $f(\zeta) = 1-(1-\zeta)^{10}$ and $g(\zeta) = \Theta(\zeta-0.5)\cdot\Theta(1-\zeta)$ by means of $p_2(\zeta)\ldots p_5(\zeta)$. Setting $f(\zeta) = a_j p_j(\zeta)$

and $g(\zeta) = b_j p_j(\zeta)$, multiplying these expansions by $p_k(\zeta)$ and integrating over ζ from 0 to 1, we obtain the expansion coefficients a_j, b_j thanks to the orthonormality of the basis functions:

$$\begin{array}{cccccc} & p_2 & & p_3 & p_4 & p_5 \\ f(\zeta) & 0.8937 & & 0.2934 & 0.0967 & 0.0327 \\ g(\zeta) & 0.6276 & & -0.2434 & -0.0720 & 0.1192 \end{array} \tag{35}$$

The plot of the resulting approximations together with the original functions in fig. 2 shows that four basis functions cannot work miracles, but reproduce the general shape in a reasonable way.

In this example, the four basis functions were chosen by appealing to the general properties of velocity profile functions in flows without slip at the bed and a stress-free upper surface. If these assumptions are not fulfilled or another physical variable like the particle concentration should be approximated, we have to choose different basis functions. In this case, the shifted Legendre polynomials may be a better choice:

$$\bar{P}_0(\zeta) = 1 \tag{36}$$
$$\bar{P}_1(\zeta) = \sqrt{3}\,(1 - 2\zeta) \tag{37}$$
$$\bar{P}_2(\zeta) = \sqrt{5}\,(1 - 6\zeta + 6\zeta^2) \tag{38}$$
$$\bar{P}_3(\zeta) = \sqrt{7}\,(1 - 12\zeta + 30\zeta^2 - 20\zeta^3) \tag{39}$$

2.4.3 Trigonometric functions

Let us now investigate sine functions with 0, 1, 2, ... nodes and the wave length corresponding to 4/1, 4/3, 4/5, ... of the flow depth:

$$\phi_j(\zeta) = \sqrt{2}\sin\left(\frac{\pi}{2}(2j+1)\zeta\right), \quad j = 0, 1, 2, \ldots. \tag{40}$$

They fulfil the same boundary conditions at the bed and at the surface as the polynomials suitable for representing velocity when there is no slip at the bed and the surface is stress-free. The first four functions are plotted in fig. 3. Expansion of the two functions $f(\zeta)$ and $g(\zeta)$ defined previously gives the approximations shown in fig. 4, obtained from the following coefficients:

$$\begin{array}{cccccc} & \phi_0 & & \phi_1 & \phi_2 & \phi_3 \\ f(\zeta) & 0.8837 & & 0.2552 & 0.1184 & 0.0613 \\ g(\zeta) & 0.6366 & & -0.2122 & -0.1273 & 0.0909 \end{array} \tag{41}$$

The approximation is somewhat better than with polynomials, especially for the power-law function. For the step function, the overshoots are similar, but there are only four instead of five intersections with the full curve.

2.5 The simplest model: infinite-slope approximation

In order to study the numerical technique in its purest form, the infinite-slope approximation seems to be ideally suited: All gradients in the x-direction vanish so that the problem reduces to one spatial and one time dimension before depth integration. With depth averaging, one obtains a slab model with predetermined shear profile, whereas MWR allows the slab to adjust its internal shearing to the distribution of forces. We can then use both the existing slab models and `entrain1d` (Issler & Pastor Pérez, 2011) in non-entraining mode for comparison.

The infinite-slope approximation simplifies the $2n + 1$ equations (12) and (25) for h and u_j radically: Equation (12) can be dropped because $h = cst$. In the remaining n equations for the u_j, only three terms survive:

$$\frac{\mathrm{d}v_i}{\mathrm{d}t} = a_i g_x + c_{ij}\frac{\nu}{h^2}v_j, \tag{42}$$

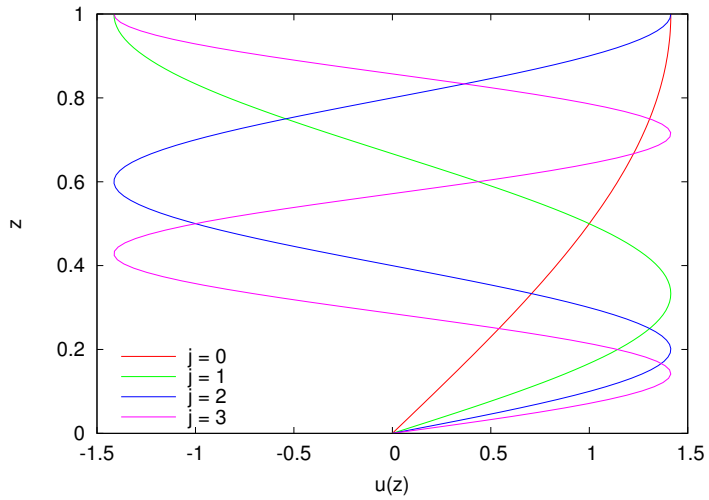

Figure 3: The first four functions of the trigonometric basis.

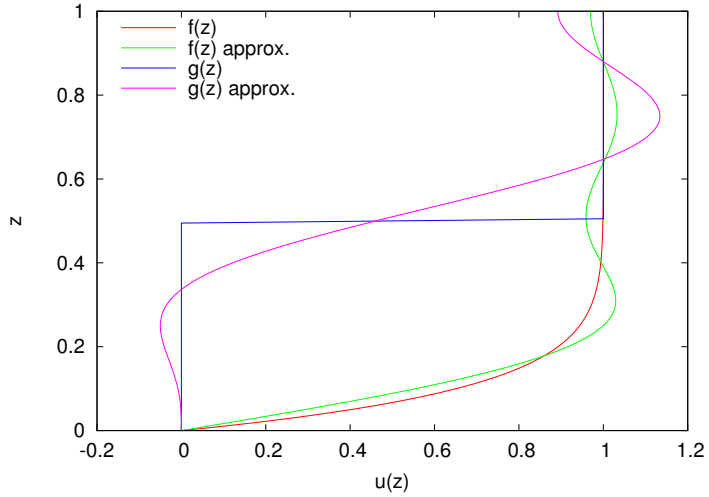

Figure 4: Two selected functions and their approximation by superpositions of the harmonics $\sqrt{2}\sin(\frac{\pi}{2}(2j+1)\zeta)$, with $j = 0, 1, 2, 3$.

and only the coefficients a_i and c_{ij} need to be calculated.

We choose $n = 4$ in the hope that this will suffice to show improvement over a simple slab model, and compare the polynomials of second to fifth order with the four sine-functions introduced earlier. The values of the coefficients a_i and c_{ij} are collected in Table 1. For the sine-basis functions, the coefficients c_{ij} with $i \neq j$ vanish because the second derivative of the basis function is proportional to the basis function itself and orthogonal to all other basis functions. The polynomials do not have this property, hence there is coupling between the different modes.

In the sine-basis, the equations decouple and can be solved immediately:

$$v_i(t) = \frac{a_i h^2 g_x}{-c_{(ii)}\nu} + \left(v_i(0) - \frac{a_i h^2 g_x}{-c_{(ii)}\nu} \right) e^{c_{(ii)}\nu t/h^2}. \tag{43}$$

Considering a viscous sheet starting from rest on an infinite incline and truncating the expansion after the first four terms, one sees that the higher modes decay much faster to their asymptotic value than the lowest mode. The asymptotic velocity, u_∞, is given by

$$u_\infty(\zeta) \approx \frac{\sqrt{2}h^2 g_x}{\nu} \sum_{j=1}^{4} \frac{a_j}{-c_{(jj)}} \sin\left(\frac{\pi}{2}(2j+1)\zeta\right).$$

Table 1: Kantorovich coefficients in the infinite-slope approximation for the case $n = 4$, for polynomial and trigonometric basis functions.

Basis	i	a_i	c_{i0}	c_{i1}	c_{i2}	c_{i3}	c_{i4}	c_{i5}
Polynomials	2	0.9129			−2.5000	−0.8204	−0.4858	−0.3371
	3	0.2996			−0.8204	−23.531	−7.3017	−7.8480
	4	0.1774			−0.4858	−7.3017	−68.469	−20.608
	5	0.1231			−0.3371	−7.8480	−20.608	−142.30
Trigonometric	0	0.9003	−2.4674	0	0	0		
	1	0.3001	0	−22.207	0	0		
	2	0.1801	0	0	−61.685	0		
	3	0.1286	0	0	0	−120.90		

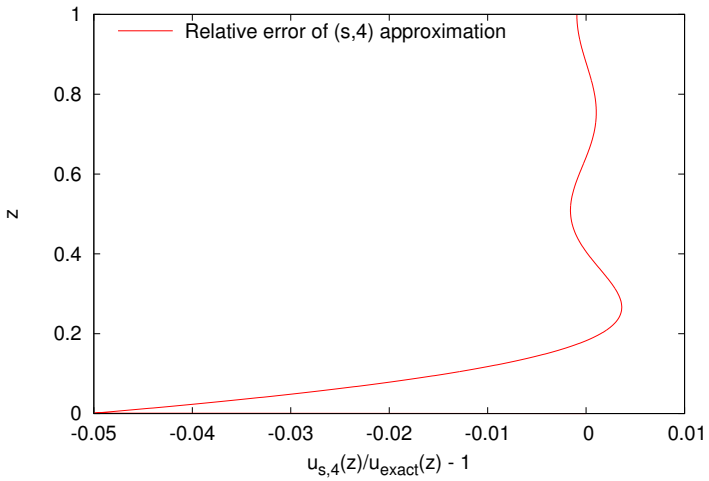

Figure 5: Relative error of the asymptotic profile function approximated with the four lowest modes of the sine-basis.

With a finite number of these basis functions, we cannot recover the exact asymptotic profile function. The relative error of the asymptotic solution is shown in fig. 5; except at the very bottom, where the velocity is small, it is well below 1%. The depth-averaged velocity, $\bar{u}(t)$, evolves towards $0.9997\,\frac{h^2 g_x}{3\nu}$, to be compared to the result from the slab model, $\bar{u}_\infty = \frac{g_x h^2}{3\nu}$, which coincides with the exact result. Within rounding errors of this calculation, the exact result for $\bar{u}_\infty$ is thus recovered.

The time evolution of the standard slab model is readily obtained as

$$\bar{u}_{\mathrm{slab}}(t) = \bar{u}_\infty \cdot \left(1 - e^{-g_x t/\bar{u}_\infty}\right). \tag{44}$$

For definiteness in the comparison, let us choose the velocity scale as $\bar{u}_\infty = 1\,\mathrm{m/s}$ and the time scale as $T = \bar{u}_\infty/g_x = \frac{h^2}{3\nu} = 1\,\mathrm{s}$. The exact solution for $\bar{u}(t)$ was approximated once by summing the first four terms of the Fourier expansion in terms of our basis functions, and once with 10,000 terms. The plotted results are indistinguishable to the naked eye, but they differ noticeably from the slab-model approximation: In the early acceleration phase, the true profile is more concave than the parabolic approximation, with an accordingly larger ratio $h\dot{\gamma}/\bar{u}$ near

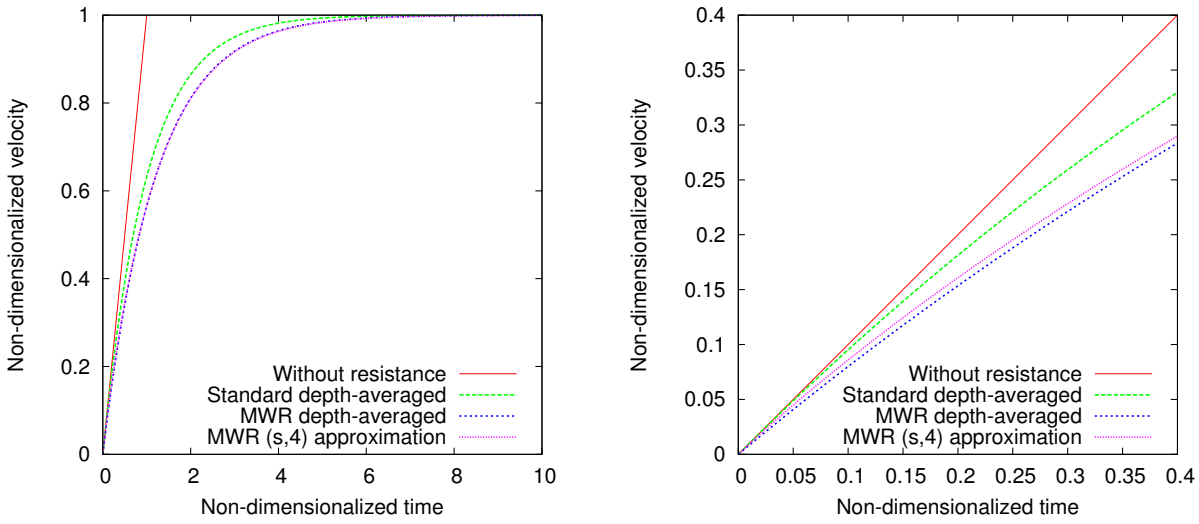

Figure 6: Comparison of the time evolution of the depth-averaged velocity between the standard slab model, the slab model derived with the MWR, and the fourth-order expansion in the sine-basis. The latter gives results that are visually indistinguishable from the exact solution.

the bed. This means that the bed shear stress is larger than in the slab model and that the slab model accelerates too rapidly, as shown in fig. 6. Interestingly, the modified slab model, derived in sec. 2.5 by using a quadratic velocity profile and weighting function, also gives results that are nearly indistinguishable from the complete solution except in the very early acceleration phase.

The evolving shape of the approximate velocity profile is shown in fig. 7 (left panel), with all profiles scaled by their surface velocity. At very early times, the exact velocity profiles are even more concave than the truncated basis functions can reproduce. This results in significant overshoots; however, they are very small on the scale of the asymptotic velocity.

Now we turn to the polynomial approximation. The evolution of the expansion coefficients v_i does not decouple in the chosen basis, but the matrix of $f_{i,j}$ is symmetric, $f_{i,j} = f_{j-2,i+2}$, and can be diagonalized. Those eigenmodes evolve independently of each other. Since such diagonalization will not generally be possible in more complicated systems, we solve the equations (42) as a coupled initial-value problem with the same velocity and time scales as for the sine-basis. Scaling the time and the expansion coefficients as $t = T\tau$ and $v_i(t) = \bar{u}_\infty v_i(\tau)$, respectively, we obtain the non-dimensional equation system

$$\frac{\mathrm{d}v_i}{\mathrm{d}\tau} = a_i + \frac{c_{ij}}{3} v_j, \tag{45}$$

which can be solved numerically (fig. 7, right panel). While the evolution of the profile shape shows the same overshoots at early times as in the sine-basis, the relaxation to the equilibrium velocity profile is about an order of magnitude slower.

The simple examples discussed in this section illustrate the following points: (i) The MWR can be successfully applied to simple flow problems with reasonable computational effort, but it requires a significant extra effort in deriving the appropriate equations. (ii) The MWR models produce results that have the correct asymptotic behavior if appropriate basis and weight functins are chosen. (iii) The MWR depth-integrated models predict the time evolution much better than the standard depth-integrated model. This is due to a more accurate description of the evolving shear layer.

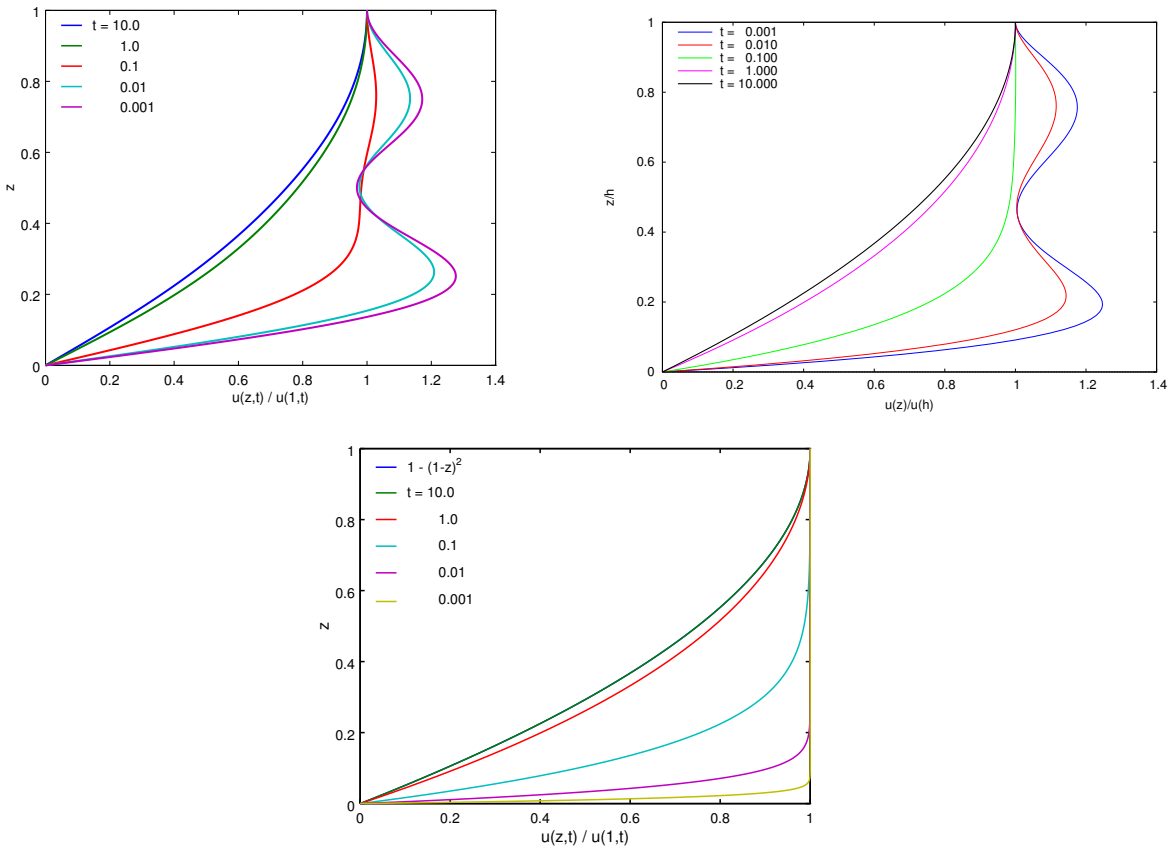

Figure 7: Evolution of the normalized profile function with time for the fourth-order approximations in the sine-basis (left panel) and polynomial basis (right panel). For comparison, the bottom panel shows the exact solution. For $t = 10$, it coincides visually with the asymptotic parabolic profile. For $t < 0.1$, neither approximation is capable of reproducing the bluntness of the exact solution, but for $t \geq 0.1$, the agreement is quite good.

3 The mathematical model for sediment flows

3.1 Balance equations

Our starting point for developing the governing equations of the sediment-flow system are the separate mass and momentum balances for the sediment (subscript s, intrinsic density $\hat{\rho}_s$) and the pore water (w, intrinsic density $\hat{\rho}_w$). For subaqueous flows, we may assume saturation and introduce the volume concentration of sediment, $0 \leq c < 1$; the volume concentration of pore water is then $1 - c$. In the mixture, the density of the sediment component is $\rho_s = c\hat{\rho}_s$ and the density of the water component is $\rho_w = (1 - c)\hat{\rho}_w$. The mixture density is

$$\rho = \rho_s + \rho_w = \hat{\rho}_w + c\Delta\hat{\rho}, \tag{46}$$

where $\Delta\hat{\rho} \equiv \hat{\rho}_s - \hat{\rho}_w$. The two components each have their own velocity, $\boldsymbol{u}_s$ and $\boldsymbol{u}_w$. The Favre-averaged mixture velocity is

$$\boldsymbol{u} = \frac{1}{\rho}(\rho_w \boldsymbol{u}_w + \rho_s \boldsymbol{u}_s). \tag{47}$$

Introducing the slip velocity,

$$\boldsymbol{w} \equiv \boldsymbol{u}_s - \boldsymbol{u}_w, \tag{48}$$

we can express $\boldsymbol{u}_s$ in terms of $\boldsymbol{u}$ and $\boldsymbol{w}$:

$$\boldsymbol{u}_s = \boldsymbol{u} + \frac{\rho_w}{\rho}\boldsymbol{w} = \boldsymbol{u} + \frac{1-c}{1+Rc}\boldsymbol{w}, \tag{49}$$

with $R \equiv \Delta\hat{\rho}/\hat{\rho}_w$.

The mass balance equations are

$$\partial_t \rho_s + \nabla \cdot (\rho_s \boldsymbol{u}_s) = 0, \tag{50}$$

$$\partial_t \rho_w + \nabla \cdot (\rho_w \boldsymbol{u}_w) = 0, \tag{51}$$

but it will be more convenient to express them as the mixture mass balance [i.e., the sum of eqns. (50) and (51)] and the balance equation of the sediment concentration,

$$\partial_t \rho + \nabla \cdot (\rho \boldsymbol{u}) = 0, \tag{52}$$

$$\partial_t c + \nabla \cdot (c \boldsymbol{u}_s) = 0. \tag{53}$$

From these equations, one sees that the component velocity fields and the mixture velocity field are divergence-free in general only if there is no relative motion between the components. However, if we defined $\boldsymbol{u}' \equiv (1-c)\boldsymbol{u}_w + c\boldsymbol{u}_s$ instead of Favre-averaging, $\nabla \cdot \boldsymbol{u}' = 0$. The price to pay for this would be additional terms in the mixture momentum balance, however.

Throughout this report, we assume that the Stokes number of the sediment particles is sufficiently low, i.e., they equilibrate to their terminal settling velocity at timescales shorter than the timescale of the flow. The differential settling velocity $\boldsymbol{w}$ will then point in the direction of the gravitational acceleration, characterized by the unit vector $\hat{\boldsymbol{g}} \equiv \boldsymbol{g}/|\boldsymbol{g}|$, and be a function of the sediment concentration: $\boldsymbol{w} = w(c)\hat{\boldsymbol{g}}$. Now we can insert eq. (47) in the equation for the divergence-free velocity $\boldsymbol{u}'$ to obtain the divergence of $\boldsymbol{u}_s$ (after a little algebra) and the advection equation for c in the form

$$\partial_t c + \left[\boldsymbol{u} + \left(\frac{1-2c-Rc^2}{1+Rc}w(c) + (1-c)cw'(c)\right)\boldsymbol{g}\right] \cdot \nabla c = 0. \tag{54}$$

The momentum balance equations for the components read

$$\partial_t(\rho_s \boldsymbol{u}_s) + \nabla \cdot (\rho_s \boldsymbol{u}_s \boldsymbol{u}_s) = \rho_s \boldsymbol{g} - \nabla p_s + \nabla \cdot (\boldsymbol{\sigma}_s + \boldsymbol{\sigma}_{ws}), \tag{55}$$

$$\partial_t(\rho_w \boldsymbol{u}_w) + \nabla \cdot (\rho_w \boldsymbol{u}_w \boldsymbol{u}_w) = \rho_w \boldsymbol{g} - \nabla p_w + \nabla \cdot (\boldsymbol{\sigma}_w + \boldsymbol{\sigma}_{sw}). \tag{56}$$

Again, we can add the equations and obtain the momentum balance of the mixture. Note that the inter-component stresses $\boldsymbol{\sigma}_{sw} = -\boldsymbol{\sigma}_{ws}$ cancel out:

$$\partial_t(\rho \boldsymbol{u}) + \nabla \cdot (\rho \boldsymbol{u}\boldsymbol{u}) = \Delta\rho \boldsymbol{g} - \nabla p + \nabla \cdot \boldsymbol{\sigma}. \tag{57}$$

Here, we removed the hydrostatic part in the pressure gradient and the body force terms so that only the dynamically relevant buoyancy forces remain: $\Delta\rho \equiv \rho - \hat{\rho}_w = c\Delta\hat{\rho}$, $p \equiv p_s + p_w - p_{\text{hydrostatic}}$. It is possible to combine eqns. (55) and (56) in such a way as to obtain a dynamical equation for the slip velocity $\boldsymbol{w}$, with the inter-component stresses playing a decisive role. However, our assumption of low Stokes number and a concentration-dependent settling velocity can be viewed as an approximate solution of that equation and obviates the need for treating it explicitly.

Note that we assume the density of the ambient water to be constant along the path of the sediment flow. In reality, there can be substantial density differences due to temperature and/or salinity differences. This simplifying assumption therefore restricts the model to applications in well-mixed domains. However, it would not be difficult to modify the model to take into account variable density of the ambient water.

The flows we will consider are characterized by an interface between the bed and the flow, located at $b(x, y, t)$, and an interface between the flow and the ambient water at $s(x, y, t)$, both quantities being measured perpendicular to the original sea floor. The flow equations will therefore be solved in the variable domain $\mathcal{D} = \{(x, y, z, t)|(x, y) \in \mathcal{D}_t \wedge t \in [T_i, T_f] \wedge z \in [b(x, y, t), s(x, y, t)]\}$. T_i and T_f are the starting and ending time of the simulation, respectively, $\mathcal{D}_t$ is a (simply-connected) fixed domain in the base surface $z = 0$. Evolution equations for b and s will be derived in sec. 3.3.

3.2 Constitutive equations

The next step is to specify explicit expressions for the settling velocity, the pressure and the stress tensor.

Settling velocity: For $\boldsymbol{w}$, we follow Sassa & Sekiguchi (2010) and use the well-tested empirical formula by Richardson & Zaki (1954):

$$w(c) = (1 - c)^n w_t, \tag{58}$$

where w_t is the settling velocity of an isolated particle far from other particles or walls. The exponent n depends on particle size and shape. According to Baldock *et al.* (2004), it can be determined experimentally by comparing w_t to the threshold velocity w_f for fluidization of a bed made of the same particles with a packing concentration c_*:

$$n = \frac{\ln(w_f/w_t)}{\ln(1 - c_*)}. \tag{59}$$

This formulation was tested in particular for coastal sands.

Pressure: Inside the flow, the MWR opens for the possibility of going beyond the hydrostatic approximation that is fundamental in depth-averaged models. This means that the effect of bed-normal acceleration is not neglected. In this case, there is a dynamical momentum balance equation in the z-direction instead of the algebraic equation balancing only pressure and gravitational force. This is of importance in strongly rotational flows like turbidity currents (see (McElwaine, 2005) for a derivation of the pressure distribution in the head of an idealized gravity current). The thin, laminar sediment flows we concentrate on in this report should, however, be adequately describable in the hydrostatic approximation. The z-component of the momentum balance then reduces to

$$p(z) \approx -\int_z^s \Delta\hat{\rho} g_z c(z')\mathrm{d}z' \tag{60}$$

if we also neglect the divergence of normal-stress differences (which would contribute to $\partial_z \sigma_{zz}$ and shear-stress gradients acting on bed-normal planes ($\partial_x \sigma_{zx}$ and $\partial_y \sigma_{zy}$).

In the bed, excess pore pressure is an important factor because it is decisive for the soil stability. The sudden pressure rise in the bed due to the rapid loading by the gravity mass flow flowing over the ground is likely the reason for the enormous erosional capacity of some debris flows. For snow avalanches, Gauer & Issler (2004) conjectured that the sudden creation of excess pore pressure in the snow cover at the front of rapid dense avalanches may lead to eruptive erosion at the very front. However, our focus here is on sedimentation and we will simply assume that the vertical pore pressure gradient is large enough to prevent fluidization of the bed, i.e., flow of water into the bed. With this assumption, we do not need to explicitly calculate the dynamics of the bed except for the deposition rate. At a later stage, it will be of interest to extend the model to cover excess pore pressure dynamics in the bed, however.

For the **deviatoric stresses**, we need to distinguish three regions: Inside the bed, we consider the material to be solid and stable against erosion or sliding. This implies that we do not need to consider its internal dynamics (consolidation, etc.), but treat it as a static layer except for its height changing in time due to sedimentation. The sedimentation rate enters as a boundary condition (see sec. 3.3).

In the liquefied layer, the effective pressure is zero and the sediment–water mixture behaves like a fluid. At low to moderate solid concentration, we may assume particle collisions to be relatively unimportant so that the slurry behaves as a Newtonian fluid with a viscosity that depends sensitively on particle concentration. Mueller *et al.* (2010) give a comprehensive review of earlier work on the rheology of dilute to concentrated suspensions of spherical and non-spherical particles and compare those results to their own extensive set of measurements. The key results can be summarized as follows:

- Newtonian behavior is a good approximation for $c \lesssim 0.25$, but the dependence of the viscosity on c deviates strongly from the linear increase deduced by Einstein for very dilute suspensions.
- The simplest satisfactory fit of the concentration dependence is provided, in the Newtonian regime, by
$$\eta(c) = \eta_0 \left(1 - \frac{c}{c_*}\right)^{-2}, \tag{61}$$
where η_0 is the dynamic viscosity of the carrier fluid and c_* the maximum packing concentration of a sheared suspension, typically in the range 0.61–0.64.
- At particle volume concentrations above 0.25, non-Newtonian effects become noticeable, among them shear-thinning with a concentration-dependent flow index $n(c) < 1$ when fitted to a Herschel–Bulkley model and the emergence of a small but finite yield strength.

These findings indicate that the assumption of a purely Newtonian fluid is not very good in a large part of the flow domain and that (possibly fluid-mediated) particle-particle interactions should be included in the rheological model.

Cassar *et al.* (2005) investigated very dense granular flows in water and found them to be describable by the same $\mu(I)$ rheology (Pouliquen & Forterre, 2002; Jop *et al.*, 2006) as dense dry granular flows. The stress tensor is

$$\sigma_{ij} = P\left(\delta_{ij} + \mu(I)\frac{2D_{ij}}{\dot{\gamma}}\right), \tag{62}$$

with P the confining pressure, $D_{ij} \equiv \frac{1}{2}(\partial_i u_j + \partial_j u_i)$ the strain-rate tensor, $\dot{\gamma} \equiv (2D_{ij}D^{ij})^{1/2}$ the second invariant of D_{ij}. The friction coefficient depends on the inertial number, I as

$$\mu(I) = \mu_s + \frac{\mu_\infty - \mu_s}{1 + I_0/I}, \tag{63}$$

where μ_s and μ_∞ are the values of the friction coefficient in the static and infinite-shear-rate limits, respectively. I is the ratio of the timescales for a particle of diameter d falling into the hollow between neighboring particles, $\tau_p = d(\hat{\rho}_s/P)^{1/2}$ in the case of dry granular flows, and the macroscopic shear, $\tau_f = 1/\dot{\gamma}$. I_0 is a material-specific constant of the order of 0.3–0.5.

Cassar *et al.* (2005) propose to modify the expression for τ_p for subaqueous flows to take into account the damping effect of the interstitial fluid. To this end, they distinguish three different regimes, following Courrech du Pont *et al.* (2003): inertial, viscous and free-fall, the latter being very similar to the situation in a dry granular flow. The criteria for separating the regimes are the Stokes number and the particle–fluid density ratio modified by the drag coefficient, $r \equiv \left(\frac{\hat{\rho}_s}{C_D\hat{\rho}_w}\right)^{1/2}$. Their experiments in water and air cover the viscous and free-fall regimes, respectively, whereas Courrech du Pont *et al.* (2003) covered the free-fall regime and the transition from the viscous to the inertial regime.

Based on typical values for sand in water ($d \approx 3\cdot10^{-4}\,\mathrm{m}$, $\hat{\rho}_s/\hat{\rho}_w \approx 2.5$, $w \approx 2\cdot10^{-2}\,\mathrm{m\,s^{-1}}$), we obtain $\mathrm{Re}_p \approx 6$, $C_D \approx 6$, $r \approx 0.6$–0.7, and $\mathrm{St} \gtrsim 1$. This indicates our system should be in

the inertial regime, but not very far from the viscous regime and possibly also fairly close to the free-fall regime. For the inertial regime, Cassar *et al.* (2005) give the following modified expression for the inertial number:

$$I = \dot{\gamma} d \left[\frac{2}{3} \frac{C_D \hat{\rho}_w}{P} \right]^{1/2} . \tag{64}$$

The pressure varies with depth in the flow basically as $(h-z)\delta\rho$, thus $I(z) \sim (h-z)^{-1/2}\dot{\gamma}$ and $\dot{\gamma}(z) \sim (h-z)^{1/2}$ in a stationary flow on an inclined plane. This leads to the well-known velocity profile of dilute granular flows on an incline,

$$u(z) = u(h) \left[1 - (1 - z/h)^{3/2} \right] . \tag{65}$$

It is, however, questionable whether this rheology for very dense granular flows is applicable to the liquefied region of the sediment flows we are interested in.

3.3 Initial and boundary conditions

The initial conditions include the initial flow depth distribution, $h_0(x, y)$ over the computational domain, the sediment concentration and the velocity vector expressed in terms of the coefficients of the basis functions, $c_{k,0}(x, y)$, $u_{k,0}(x, y)$ and $v_{k,0}(x, y)$ for $k = 0, 1, \ldots, N$—to be discussed in depth in sec. 4.

Location of moving boundaries. Our problem contains moving interfaces and boundaries, both at the upper surface of the flow towards the ambient fluid, $s(x, y, t)$, and at the bottom of the flow towards the bed at rest, $b(x, y, t)$. In a vertically resolved model like LIQSEDFLOW, the location of these boundaries is a result of solving the flow equations in the entire domain and tracking the evolution of the interface by means of a suitable technique like Volume of Fluid (VoF). The same can in principle be done with MWR, but obtaining good approximations for functions with discontinuities at these interfaces would require the use of a large number of basis functions. It therefore appears more useful to use basis functions in the variable interval $[b(x, y, t), s(x, y, t)]$. It is therefore necessary to obtain additional equations describing the evolution of b and s. This can be achieved in the following way.

The upper surface is material with respect to the particles. Therefore, the kinematic boundary condition

$$\partial_t s + \left[\boldsymbol{u}_{s\parallel} \cdot \nabla_\parallel \right]_{z=s} = \boldsymbol{u}_s|_{z=s} \cdot \hat{\boldsymbol{z}} \tag{66}$$

must hold. The $\parallel$ subscript indicates that only the vector components in the local tangential plane to the bathymetry should be used. $\hat{\boldsymbol{z}}$ is the unit vector along the local z-direction. In eq. (66), $\boldsymbol{u}_s$ should be expressed in terms of the volume-averaged velocity $\boldsymbol{v}$ and the hindered settling velocity $\boldsymbol{w} = w(c)\hat{\boldsymbol{g}}$:

$$\partial_t s + \left[\boldsymbol{v}_\parallel + (1-c) w(c) \hat{\boldsymbol{g}}_\parallel \right]_{z=s} \cdot \nabla_\parallel s = \left[\boldsymbol{v} + (1-c) w(c) \hat{\boldsymbol{g}} \right]_{z=s} \cdot \hat{\boldsymbol{z}} \tag{67}$$

Approximate values of the velocity $\boldsymbol{v}$ at $z = b, s$ are accessible in the MWR. Note that the concentration may be discontinuous at $z = s$, and both $\boldsymbol{u}_s$ and $\boldsymbol{u}_w$ have discontinuities proportional to Δc, but the volumetric mixture is continuous across the boundary.

The interface to the bed is not a material boundary, but must be treated as a shock front in terms of the particle concentration and velocity (and the water velocity). The material in the bed is at rest in the laboratory frame. The sediment flux across the interface can thus be expressed as

$$c|_{z=b_+} (\boldsymbol{u}_s|_{z=b_+} \cdot \hat{\boldsymbol{n}} - \partial_t b) = -c_* \hat{\boldsymbol{n}} \cdot \hat{\boldsymbol{z}}\, \partial_t b, \tag{68}$$

where $\hat{\boldsymbol{n}}$ is the unit normal vector to the interface, pointing into the flow, and c_* is the particle concentration in the bed, assumed to correspond to densest random packing. The notation

$z = b_+$ indicates that the fields are to be evaluated just above the interface. The corresponding equation for the water flow results from exchanging c (c_*) by $1 - c$ ($1 - c_*$) and $\boldsymbol{u}_s$ by $\boldsymbol{u}_w$. Adding these two equations and using the definition of $\boldsymbol{v}$, one confirms that $\boldsymbol{v} \cdot \hat{\boldsymbol{n}} = 0$. (If one assumes that the water obeys the no-slip condition at the interface, the mixture velocity does have a tangential component at $z = b$ unless $\boldsymbol{w}$ and $\hat{\boldsymbol{n}}$ are parallel.) Again, we substitute for $\boldsymbol{u}_s$ in terms of $\boldsymbol{v}$ and $\boldsymbol{w}$ and solve for $\partial_t b$, making use of $\boldsymbol{v} \cdot \hat{\boldsymbol{n}} = 0$:

$$\partial_t b = -\left.\frac{c}{c * -c}\right|_{z=b_+} \boldsymbol{u}_s|_{z=b_+} \cdot \hat{\boldsymbol{n}} = -\left.\frac{(1-c)cw(c)}{c_* - c}\right|_{z=b_+} \hat{\boldsymbol{g}} \cdot \hat{\boldsymbol{n}}. \tag{69}$$

Stress boundary condition. We are, at this point, not attempting a fully coupled formulation that takes into account the motion of the ambient fluid, which would enable us to compute the generation of a tsunami due to a submarine landslide. Instead, we approximate the effect of the ambient fluid on the flow in a rough way by means of a stress boundary condition at the upper surface of the flow, in the same way as done, e.g., by De Blasio *et al.* (2004): The drag force is assumed proportional to the square of the velocity and the area measured parallel to the bed, with the drag coefficient C_D consisting of a frictional part, C_f, depending on the roughness of the flow surface and a pressure part, C_p, associated with the frontal area exposed to the flow. This is formulated mathematically as follows:

$$\sigma_{xy}^{(s)} = -\frac{C_D}{2}\hat{\rho}_w |\boldsymbol{u}^{(s)}| \boldsymbol{u}^{(s)}, \tag{70}$$

$$C_D = C_f - C_p \boldsymbol{c} \cdot \nabla_t h \Theta(-\boldsymbol{c} \cdot \nabla_t h). \tag{71}$$

The operator ∇_t is the gradient operator restricted to the local tangent plane to the bed, $\Theta(x) = 1$ for $x > 0$ and 0 otherwise, and $\boldsymbol{c}$ is the unit vector parallel to the surface velocity $\boldsymbol{u}^{(s)}$. Thus the pressure drag is modeled to act only on sloping areas of the flow surface facing in the flow direction, and force components perpendicular to the flow direction are neglected. Despite its shortcomings, this formula captures the essence of a process that is neglected in the majority of similar models, yet has a strong influence on the velocity for large flows.

The pressure drag coefficient, C_p, is expected to lie somewhere between that of a blunt body with $C_p = \mathcal{O}(1)$ and that of a streamlined object with $C_p = \mathcal{O}(0.01 \ldots 0.1)$. The value to be used in the simulation is selectable by the user and written in the input file.

The value of the coefficient C_f should be close to that of a flat plate of the same length L and roughness R. The relevant dimensionless parameters are the Reynolds number, $\mathrm{Re} \equiv UL/\nu_w$, and the ratio of roughness length to flow length, $r \equiv R/L$. In typical submarine sediment flows, they take values of the order of $\mathrm{Re} \sim 10^7 \ldots 10^10$ and $r \sim 10^{-6} \ldots 10^{-4}$, respectively, but in submarine debris flows carrying large clasts, r may be several orders of magnitude larger. In the laboratory, typical values are $\mathrm{Re} \sim 10^4 \ldots 10^6$ and $r \sim 10^{-4} \ldots 10^{-2}$, respectively. Based on these numbers, the boundary layer will be turbulent and one could use the customary expression

$$C_f = 0.0594 \left(\frac{\nu_w}{\ell u^{(s)}}\right)^{0.2},$$

where ℓ is the distance from the front of the sediment flow to the point under consideration, measured along the streak lines. However, we anticipate that it will be difficult to evaluate ℓ in an Eulerian code, and we therefore resort to a constant value, to be selected by the user before the simulation, in the range $0.001 < C_f < 0.01$.

Equation (70) provides one of the two required boundary conditions for the velocity. The other is the no-slip condition at the interface with the bed, $\boldsymbol{u}(x, y, 0, t) = \boldsymbol{0}$. As will be seen in sec. 4, this condition is implemented by choosing basis functions that vanish identically at $z = 0$.

The transport equation for the sediment concentration is a first-order differential equation as long as we do not take into account turbulent mixing at the upper surface. Thus, we need

to provide one boundary condition. The value at the upper surface is not determined, nor is the value at the interface to the bed. We can, however, formulate a condition derived from the conservation of mass across the moving interface:

$$\frac{\mathrm{d}b}{\mathrm{d}t}(x,y,t) = \frac{c^+(x,y,t)}{c_b} w^+(x,y,t), \tag{72}$$

where both $c^+(x,y,t) \equiv c(x,y,0^+,t)$ and $w^+(x,y,t) \equiv w(c(x,y,0^+,t))$ are to be evaluated just above the interface. ρ_b is the density of the bed, assumed constant in time and space. In a similar way, the kinematic boundary condition at the upper flow surface ensures that no sediment flows across that surface.

4 Application of the method of weighted residuals to sediment flows

4.1 Brief overview of the method

The fields in our model are elements of a function space over a given spatio-temporal domain $\mathcal{D}$, which we may decompose as $\mathcal{D} = \mathcal{M}_2 \times [0,H] \times \mathbb{R}_+$. $\mathcal{M}_2$ is a real two-dimensional bounded manifold, representing the bathymetry of the area in which the flow develops. We assume the flow volume to be bounded in height (measured perpendicularly to the sea floor), with H smaller than the minimum radius of curvature in $\mathcal{M}_2$. $\mathbb{R}_+$ is the set of non-negative real numbers, representing time from the start of the flow at $t = 0$.

For the time being, we assume the fields to be twice continuously differentiable on $\mathcal{D}$ and to possess a finite L_2 norm in $\mathcal{M}_2 \times \mathbb{R}_+$. More precisely, the integral

$$\langle \Phi_a, \Phi_b \rangle(t) \equiv \int_{\mathcal{M}_2} \int_0^H \Phi_a(x,y,z,t) \Phi_b(x,y,z,t) \,\mathrm{d}z \,\mathrm{d}y \,\mathrm{d}x \tag{73}$$

should be supplemented by a weight $\det[G(x,y)](1+\kappa_1(x,y)z)(1+\kappa_2 z)$ to account for curvature effects of the manifold $\mathcal{M}_2$, where G_{ij} is the metric tensor on $\mathcal{M}_2$ and $\kappa_{1,2}$ are the principal curvatures. The weight factor depends on the location on $\mathcal{M}_2$, and this fact has important consequences for the further development of the mathematical framework, as will be seen below. For this reason, we neglect these corrections, i.e., set $\det(G) \approx 1$ and $\kappa_{1,2} \approx 0$.

If we choose a complete set of basis functions $\left\{ B_i^{(\Phi)}(z),\ i \in \mathbb{I} \subseteq \mathbb{Z} \right\}$ on $[0,H]$, we may expand the z-dependence of the fields in terms of these basis functions:

$$\Phi(x,y,z,t) = \sum_{i \in \mathbb{I}} \phi_i(x,y,t) B_i^{(\Phi)}(z), \tag{74}$$

where the coefficients are again fields, albeit with one dimension less. We chose the clumsy notation $B_i^{(\Phi)}$ to indicate that different sets of basis functions may be chosen for different fields Φ. In our case with $\Phi \in \{u, v, c\}$, the velocities u and v have similar properties and we will use the same basis functions for them. The sediment concentration c, however, has a strongly different profile shape so that it may be convenient to use a more adapted basis set to get a good approximation with few terms.

When this expansion is inserted into the differential equations, all z-dependence resides in the basis functions. At this stage, however, we have a large number of coefficient functions and too few equations to determine them. The next step is to choose a corresponding number of weight functions $W(z)$ with which to multiply and integrate the differential equations over z so that a larger number of lower-dimensional partial differential equations result. Those equations are then to be solved by traditional discretization techniques.

As a simple illustration, we consider a one-dimensional advection equation for a particle suspension settling under gravity, assuming a concentration-dependent settling velocity $w(C)$, i.e., hindered settling. This is the special case of our general problem where there is no flow. In the first instance, we avoid the problem of moving boundaries by assuming that there is a time-dependent supply of particles at $z = H$ and that particles arriving at $z = 0$ simply flow out of the domain. Thus the problem consists of the differential equation

$$\partial_t C + \partial_z[w(C)C] = 0, \tag{75}$$

the initial condition

$$C(z, 0) = C_0(z), \tag{76}$$

and the boundary condition

$$C(0, t) = f(t). \tag{77}$$

Finally, we assume the Richardson–Zaki formula (58) for $w(C)$, with some $n > 1$.

Particles in regions with high concentration fall less rapidly than those in dilute regions, hence there is a tendency for steepening of the concentration gradient as in shoaling waves where the propagation speed increases with wave height. This implies that a great variety of profile shapes with large gradients may occur. We conjecture that a Fourier series containing both sine and cosine terms is a reasonable choice. So we write, with $\zeta \equiv z/H$,

$$C(z) = c_0 B_0(z) + \sum_{j=1}^{\infty} \left[c_j(t) \cos(2\pi j\zeta) + s_j(t) \sin(2\pi j\zeta) \right]. \tag{78}$$

The basis functions $B_0(z) \equiv 1/\sqrt{2}$, $B_{2j-1}(z) \equiv \sin(2\pi j\zeta)$ and $B_{2j}(z) \equiv \cos(2\pi j\zeta)$, $j \in \mathbb{N}_+$, are orthonormal with respect to the scalar product

$$\langle B_i, B_j \rangle = \frac{2}{H} \int_0^H B_i(z) B_j(z) \mathrm{d}z \tag{79}$$

on $[0, H]$. The coefficients are obtained as the scalar products of the function with the basis functions:

$$c_0 = \frac{2}{H} \int_0^H C(z) \frac{1}{\sqrt{2}} \mathrm{d}z, \quad c_j = \frac{2}{H} \int_0^H C(z) \cos(2\pi j\zeta) \mathrm{d}z, \quad s_j = \frac{2}{H} \int_0^H C(z) \sin(2\pi j\zeta) \mathrm{d}z. \tag{80}$$

Our equation being non-linear, inserting the expansion requires expressing $(1 - C)^n$ as a power series in C using the binomial series,

$$(1 + x)^n = \sum_{j=0}^{\infty} \binom{n}{j} x^j \tag{81}$$

with the generalized binomial coefficients

$$\binom{n}{j} \equiv \frac{n(n-1)(n-a)\cdots(n-j+1)}{j!}. \tag{82}$$

The concentration being bounded by $C_* < 1$, the series is assured to converge, but we need high orders for the relative error to become sufficiently small at the maximum concentration of about 0.6. For the value $n = 4.65$ used by Sassa & Sekiguchi (2010), seven terms are needed:

$$w(C)C = C - 4.65\, C^2 + 8.4863\, C^3 + 7.4962\, C^4 + 3.0922\, C^5 + 0.40198\, C^6 + \mathcal{O}(C^7).$$

The next step is to substitute the expansion (78) for C, truncated to $2N + 1$ terms, in the equation above. Even with this modest requirement on the precision of the approximation

of $w(C)C$, the expansion of $w(C)C$ contains about $(2N+1)^6$ terms of products of up to six trigonometric functions. In order to reproduce the sharp boundaries reasonably, we conjecture that N should be at least 3, giving of the order of 10^5 terms or more. To tackle this task, a computer algebra system (CAS) is a prerequisite.

Once this is completed, one proceeds to obtain ODEs for the coefficient functions $c_j(t)$, $s_j(t)$ by multiplying the expanded and truncated PDE for $C(z,t)$ by suitably chosen weight functions $W_k(z)$ and integrating over z. Usually, the same number of weight functions is used as there are basis functions so that a fully determined system results. Often, the most convenient choice is to use the same functions as for the basis. With our choice of orthonormal basis functions, the first term in the integrated PDE becomes the time derivative of the coefficient of the kth basis function, $\dot{c}_k(t)$. The advection term leads to integrals of the type

$$\int_0^{2\pi} \cos^{a_1} x \cos^{a_2}(2x) \cos^{a_3}(3x) \sin^{b_1} x \sin^{b_2}(2x) \sin^{b_3}(3x)\,\mathrm{d}x$$

with $\sum_{j=1}^{3}(a_j+b_j) \le 2N+2$. They can be evaluated using standard techniques of integration, but again a CAS is needed.

From the point of view of numerical efficiency, this is a completely non-viable situation. The primary reason for its emergence is the strong non-linearity of the Richardson–Zaki correlation (58) for the settling velocity. In the other extreme of constant settling velocity, the advection equation (54) becomes linear and splits into $2N+1$ uncoupled ODEs for the coefficients $c_0, c_1, \ldots, c_N, s_1, \ldots, s_N$ if the basis functions are also used as weight functions.

4.2 Settling column with homogeneous initial condition

For the purpose of testing the potential of the MWR, we study the simpler problem of a settling experiment of suspended identical particles that are homogeneously distributed at $t=0$ with volume concentration C_0. Under these conditions, there is an analytic solution to the problem for which hindered settling does not pose problems: From the top, a rarefaction front moves downward at the settling speed $w(C_0)$, above which there are no particles. From the bottom, a shock front moves upward at a speed determined by $w(C_0)$, C_0 and the deposit concentration C_*. In the shrinking space between the two fronts, the concentration remains constant at C_0 because the influx into a reference volume matches the outflux:

$$C(z,t) = \begin{cases} 0, & H - wt \le z \le H \\ C_0, & \frac{C_0}{C_*} wt < z < H - wt \\ C_*, & 0 \le z \le \frac{C_0}{C_*} wt \end{cases} \tag{83}$$

This solution is not stable against small perturbations if w depends on C, but we circumvent this here by assuming $w = w(C_0)$. The expressions are valid in the time interval $0 \le t \le \frac{H}{w}(1 - C_0/C_*)$. Afterwards, the solution is constant in time: $C(z,t) = C_*$ for $0 \le z < HC_0/C_*$ and $C(z,t) = 0$ for $HC_0/C_* < z \le H$.

Fourier-expanding the exact solution (83) for $0 \le t \le \frac{H}{w}(1 - C_0/C_*)$, we obtain the following expressions for the coefficients:

$$\begin{aligned} c_0(t) &= \sqrt{2} C_0 \left(1 - \frac{wt}{H}\frac{C_0}{C_*}\right) \\ c_k(t) &= \frac{1}{k\pi}\left[(C_* - C_0)\sin\left(2\pi k \frac{C_0}{C_*}\frac{wt}{H}\right) - C_0 \sin\left(2\pi k \frac{wt}{H}\right)\right], \quad k \ge 1, \\ s_k(t) &= \frac{1}{k\pi}\left[C_* - (C_* - C_0)\cos\left(2\pi k \frac{C_0}{C_*}\frac{wt}{H}\right) - C_0 \cos\left(2\pi k \frac{wt}{H}\right)\right], \quad k \ge 1. \end{aligned} \tag{84}$$

As fig. 8 shows, a good approximation of this step function by a truncated Fourier series requires far more than 7 ($N=3$) or 17 terms ($N=8$).

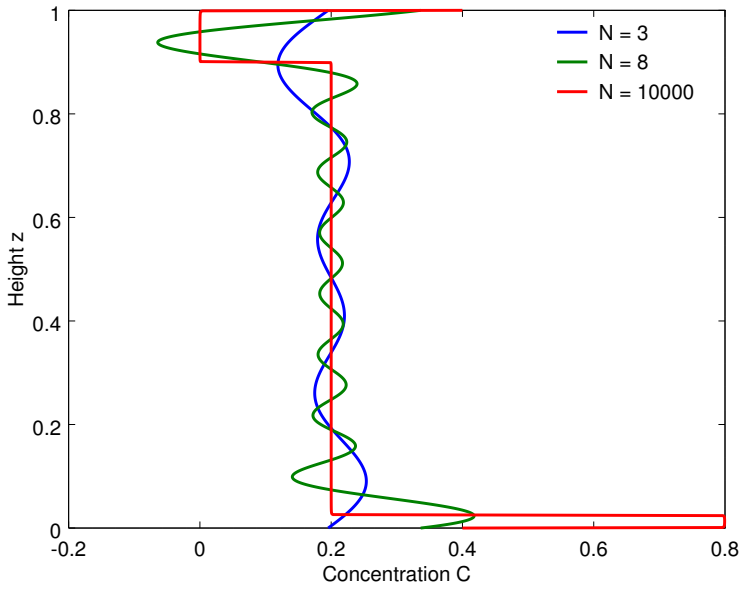

Figure 8: Approximation of the exact solution for the settling column experiment by its Fourier series truncated at different orders $N = 3, 8, 10,000$. $C_0 = 0.2$, $C_* = 0.8$, $wt = 0.1H$.

Reproducing this simplest case by the MWR will nevertheless constitute a challenge to the method because of the discontinuities at the moving boundaries. Truncating the expansion (78) at $N \geq 1$, the differential equation (54) becomes

$$\begin{aligned} \frac{\dot{c}_0(t)}{\sqrt{2}} &+ \sum_{j=1}^{N} [\dot{c}_j(t)\cos(2\pi j\zeta) + \dot{s}_j(t)\sin(2\pi j\zeta)] \\ &= 2\pi\frac{w}{H}\sum_{j=1}^{N}[-c_j(t)j\sin(2\pi j\zeta) + s_j(t)j\cos(2\pi j\zeta)] \\ &\quad + wC_0[\delta(z - wtC_0/C_*) - \delta(z - H + wt)]. \end{aligned} \tag{85}$$

At the points wtC_0/C_* and $H - wt$, $C(z)$ and the flux $w(C_0)C$ are discontinuous (even though the one-sided derivatives of $C(z)$ at these points are equal): Inside this interval, it is $-wC_0$, outside it vanishes. The discontinuities contribute $wC_0[\delta(z - wtC_0/C_*) - \delta(z - H + wt)]$ to the right-hand side of eq. (85). Note, however, that writing the ODE with the discontinuities expressed in this way already includes crucial information about the location of the shocks that should be obtained through the solution procedure.

The initial condition $C(z, 0) = C_0$ is easy to expand in terms of the basis functions—we find $c_0(0) = \sqrt{2}C_0$ and all other $c_j(0)$ and $s_j(0)$ vanish. Next, we multiply eq. (85) in turn by each of the basis functions and integrate from 0 to H, making use of the orthonormality of the chosen basis functions. This leads to the set of equations

$$\begin{aligned} \dot{c}_0 &= 0, \\ \dot{c}_j &= 2\pi j\frac{w}{H}s_j + 2C_0\frac{w}{H}\left[\cos(2\pi j\tau) - \cos(2\pi jr\tau)\right], \\ \dot{s}_j &= -2\pi j\frac{w}{H}c_j + 2C_0\frac{w}{H}\left[\sin(2\pi j\tau) + \sin(2\pi jr\tau)\right], \end{aligned} \tag{86}$$

where we defined $r \equiv C_0/C_*$ and $\tau \equiv wt/H$ and used the relations $\cos(2\pi - x) = \cos x$, $\sin(2\pi - x) = -\sin x$.

Clearly, eqns. (86) do not agree with eqns. (85). Moreover, according to eqns. (86), $\dot{c}_0(0) = \dot{c}_j(0) = \dot{s}_j(0) = 0$ because $c_j(0) = s_j(0) = 0$ and the effects of the flux discontinuities cancel due to their symmetric location at $t = 0$ with opposite signs and the vanishing of the sine basis functions at the endpoints $z = 0$ and $z = H$. So far, our efforts to understand the reason for this discrepancy have failed. The most likely reason is the formulation of the boundary or jump conditions. The exact solution (83) suggests that it will not be difficult to recover the exact solution from the evolution equation of the coefficients, once eqn. (86) is correctly deduced from the original advetion equation.

Nonetheless, fig. 8 shows that a large number of basis functions are needed for a meaningful approximation of the exact solution with shocks. This implies that the MWR approach will not bring about a substantial performance gain compared to a conventional finite-difference approach resolving the vertical dimension. In certain cases, some performance gain may be possible by choosing a truncated basis that is optimally suited to the problem. However, the settling-column problem contains many of the elements that are important in sediment flows—in particular the possibility of concentration shocks. Our attempts at finding a more suitable set of basis functions have not yielded promising results so far.

5 Outlook

At the beginning of the investigation described in this report, the MWR appeared to hold great promise as a numerical approach to modeling sediment flows. It was expected to be vastly more efficient than fully 3D models. At the same time it seemed to offer a way out of the inherent limitations that make depth-averaged sediment flow models incapable of properly describing the dynamically relevant vertical motion of suspended particles in these flows.

The first application we investigated was only meant as an exercise to get better acquainted with the method in a simple context. Indeed we found that the MWR offers interesting possibilities for capturing the transient behavior of simple gravity mass flows. The standard derivation of the depth-averaged balance equations can be viewed as a special case of the MWR: One chooses a single fixed basis function for each equation—the constant function for the mass balance and usually the function describing the shape of the equilibrium velocity profile for the momentum balance. As weighting function, the standard procedure uses the constant function for both the mass and momentum balances.

However, the theory behind the MWR suggests that the weighting functions may be chosen differently for the mass and momentum balances, thus offering a wide variety of different approximations. With a weighting function for the momentum balance equation that emphasizes the area of highest shear, one obtains non-standard coefficients for the inertial, advection and bed-friction terms, but the model retains its basic structure so that the same discretization techniques can be applied as in the standard depth-averaged model and the numerical effort remains unchanged.

Choosing the weighting function equal to the equilibrium velocity profile function, we found the asymptotic velocity on an inclined plane to be the same as in the corresponding standard depth-averaged model, but equilibrium is approached somewhat more slowly. This agrees qualitatively with the fact that the standard depth-averaged model underestimates the velocity gradient at the bed for an accelerating flow; consequently, the bed shear stress is also underestimated while the acceleration is overestimated. Our results suggest that this new approach deserves a more thorough investigation with regard to consistency and accuracy. To this end, the start-up behavior of this non-standard depth-averaged model should be compared to both the standard depth-averaged model and to an accurate depth-resolved numerical model. A related open question is to find the optimum approximation with respect to given criteria, e.g., correct asymptotic velocity and closest approximation of the start-up acceleration.

As a short-cut around such a comprehensive study and to explore further aspects of the

MWR, we simplified the problem further by discarding the gradients of the fields in the flow direction. This is known as the infinite-slope approximation in geotechnics and as mass-point models (with internal structure) in the literature on slide dynamics. An advantage of this simple setting is that analytical solutions can be found for, e.g., the motion of a laminar viscous fluid from rest to its asymptotic state. The standard depth-averaged mass-point model reproduces the asymptotic velocity correctly, but approaches it too rapidly because the shear rate and shear stress at the bed are underestimated. We formulated and solved the equations for a MWR approximation with four basis functions that fulfil the boundary conditions of the problem. We compared a polynomial basis of second to fifth order to four sine-functions and found both approximations to reproduce the full solution almost perfectly. The relative deviations are largest at very short times after start because neither of the truncated bases is able to reproduce the extreme bluntness of the exact solution to the velocity profile.

On the one hand, the polynomial basis provided a marginally better approximation of the velocity profile than the trigonometric basis. On the other hand, the modes decouple in the latter, and solving the resulting equations becomes very easy and efficient. In other problems, namely the approximation of the equilibrium velocity profile of a Bingham fluid on an inclined plane (featuring a plug-flow layer) or of a step function, evaluating the expansion coefficients was easier in the polynomial basis, but the trigonometric basis provided a better approximation. This shows clearly that there are no immediately obvious rules for choosing the basis, and the question needs to be considered separately for each case.

In summary, we think that the MWR offers some interesting perspectives in the context of essentially linear problems with smooth profile functions in the transverse direction. There is a possibility that a suitably constructed non-standard depth-averaged model for gravity mass flows captures the dynamics more accurately than standard depth-averaging, without any performance penalty. Using more than one basis function allows to capture the dynamical variation of the velocity field in the bed-normal direction, albeit at the price of increased computational effort. An interesting open question is how the quality of the approximation and the computational effort scale with the number of basis functions used.

In contrast, the prospects for applying the MWR to our main target, namely depositing sediment flows, turned out to be rather bleak. The reason for this disappointing finding is twofold, namely (i) the strong non-linearity introduced into the sediment advection equation by the concentration dependence of the settling velocity and (ii) the sharp concentration gradients that typically arise in such problems. Problem (i) leads to high powers of the concentration appearing in the equations, and problem (ii) forces the use of a large number of basis functions. These two consequences conspire to couple the modes strongly. Even if one manages to determine all the coefficients in the model equations by means of a computer algebra system, the computational effort of solving the resulting coupled system by far exceeds the one in a fully 3D CFD model.

There are nevertheless some related applications where the MWR may have a better chance of succeeding. If the sediment concentration is low enough and the settling velocity can be approximated as a constant, and furthermore if turbulent mixing smoothens the concentration gradient, the resulting equation system may be manageable and constitute an interesting alternative to simple depth-averaged models and fully 3D computational fluid dynamics codes. Such a model would have important practical applications to turbidity currents, powder snow avalanches and pyroclastic suspension flows (nuages ardentes).

Acknowledgments. This work was made possible by a JSPS Invitational Fellowship to DI, supplemented by a research stipend from NGI to DI, who very much appreciates this support. DI also wishes to thank the Port and Airport Research Institute in Yokosuka, and in particular the Soil Dynamics Group, for their kind hospitality during his fruitful and very enjoyable stay in Japan, which gave him many remembrances to treasure.

References

Baldock, T. E., Tomkins, M. R., Nielsen, P. & Hughes, M. G. 2004 Settling velocity of sediments at high concentrations. *Coast. Engng.* **51**, 91–100.

Campbell, C. S. & Gong, A. 1986 The stress-tensor in a two-dimensional granular shear flow. *J. Fluid Mech.* **164**, 107–125.

Cassar, C., Nicolas, M. & Pouliquen, O. 2005 Submarine granular flows down inclined planes. *Phys. Fluids* **17**, 103301.

Courrech du Pont, S., Gondret, Ph., Perrin, B. & Rabaud, M. 2003 Granular avalanches in fluids. *Phys. Rev. Lett.* **90** (4), 044301.

De Blasio, F. V., Elverhøi, A., Issler, D., Harbitz, C. B., Bryn, P. & Lien, R. 2004 Flow models of natural debris flows originating from overconsolidated clay materials. *Marine Geol.* **213** (1–4), 415–438.

Gauer, P. & Issler, D. 2004 Possible erosion mechanisms in snow avalanches. *Annals Glaciol.* **38**, 384–392.

Irgens, F 2004 The NIS rheological model. Talk presented at SATSIE workshop in Tyriheim, Norway, on April 19, 2004; available at http://leeds.ac.uk/satsie/private/docs.

Issler, D. & Pastor Pérez, M. 2011 Interplay of entrainment and rheology in snow avalanches: a numerical study. *Annals Glaciol.* **52** (58), 143–147.

Jop, P., Forterre, Y. & Pouliquen, O. 2006 A constitutive law for dense granular flows. *Nature* **441** (7094), 727–30.

McElwaine, J. N. 2005 Rotational flow in gravity current heads. *Phil. Trans. R. Soc. A* **363**, 1603–1623.

Mueller, S., Llewellin, E. W. & Mader, H. M. 2010 The rheology of suspensions of solid particles. *Proc. R. Soc. (London), Ser. A* **466**, 1201–1228.

Parker, G., Fukushima, Y. & Pantin, H. M. 1986 Self-accelerating turbidity currents. *J. Fluid Mech.* **171**, 145–181.

Pasquarell, G C, Ackermann, N L, Shen, H H & Hopkins, M A 1988 Collisional stress in granular flows: Bagnold revisited. *J. Eng. Mech.* **114** (1), 59–64.

Pouliquen, O & Forterre, Y 2002 Friction law for dense granular flows: application to the motion of a mass down a rough inclined plane. *J. Fluid Mech.* **453**, 133–151.

Richardson, J. F. & Zaki, W. N. 1954 Sedimentation and fluidisation: part 1. *Trans. Instn. Chem. Engnrs.* **32**, 35–53.

Ruyer-Quil, C. & Manneville, P. 1998 Modeling film flows down inclined planes. *Eur. Phys. J. B* **6** (2), 277–292.

Ruyer-Quil, C. & Manneville, P. 2000 Improved modeling of flows down inclined planes. *Eur. Phys. J. B* **15**, 357–369.

Ruyer-Quil, C. & Manneville, P. 2002 Further accuracy and convergence results on the modeling of flows down inclined planes by weighted-residual approximations. *Phys. Fluids* **14** (1), 170–183.

Sassa, S. & Sekiguchi, H. 2010 LIQSEDFLOW: Role of two-phase physics in subaqueaous sediment gravity flows. *Soils Found.* **50** (4), 495–504.

Scheid, B., Ruyer-Quil, C. & Manneville, P. 2006 Wave patterns in film flows: modelling and three-dimensional waves. *J. Fluid Mech.* **562**, 183–222.

Scheiwiller, T. 1986 Dynamics of powder-snow avalanches. PhD thesis, Laboratory of Hydraulics, Hydrology and Glaciology, ETH Zürich, Zürich, Switzerland, available from http://people.ee.ethz.ch/~vawweb/vaw_mitteilungen/081/081_g.pdf.

Scheiwiller, T. & Hutter, K. 1982 Lawinendynamik – Übersicht über Experimente und theoretische Modelle von Fliess- und Staublawinen. Mittlg. VAW 58. Laboratory of Hydraulics, Hydrology and Glaciology, ETH Zürich, Zürich, Switzerland, in German. Available from http://people.ee.ethz.ch/~vawweb/vaw_mitteilungen/058/058_g.pdf.